Journal of King Saud University – Science 34 (2022) 102028

Contents lists available at ScienceDirect

Journal of King Saud University – Science

journal homepage: www.sciencedirect.com

Original article

Synthesis of cobalt and sulphur doped titanium dioxide photocatalysts for environmental applications

Muhammad Hafeez [a], Sumera Afyaz [a], Awais Khalid [b], Pervaiz Ahmad [c,*], Mayeen Uddin Khandaker [d], Muhammad Umar Khayam Sahibzada [e], Ikhtiar Ahmad [a], Jahanzeb Khan [a], Fahad A. Alhumaydhi [f], Talha Bin Emran [g], Abubakr M. Idris [h,i]

[a] Department of Chemistry, University of Azad Jammu & Kashmir, Muzaffarabad, Azad Kashmir 13100, Pakistan
[b] Department of Physics, Hazara University Mansehra, 21300 Khyber Pakhtunkhwa, Pakistan
[c] Department of Physics, University of Azad Jammu and Kashmir, 13100 Muzaffarabad, Pakistan
[d] Center for Applied Physics and Radiation Technologies, School of Engineering and Technology, Sunway University, Bandar Sunway 47500, Selangor, Malaysia
[e] Department of Pharmacy, The Sahara College Narowal, Narowal, Punjab, Pakistan
[f] Department of Medical Laboratories, College of Applied Medical Sciences, Qassim University, Buraydah 52571, Saudi Arabia
[g] Department of Pharmacy, BGC Trust University Bangladesh, Chittagong, Bangladesh
[h] Department of Chemistry, College of Science, King Khalid University, Abha 62529, Saudi Arabia
[i] Research Center for Advanced Materials Science (RCAMS), King Khalid University, Abha 62529, Saudi Arabia

ARTICLE INFO

Article history:
Received 27 October 2021
Revised 5 April 2022
Accepted 10 April 2022
Available online 18 April 2022

Keywords:
TiO_2-nanostructures
Photocatalysts
Dyes-Degradation
Water Remediation

ABSTRACT

In this work, we report the preparation of TiO_2 and Co-S doped TiO_2 nanostructures by sol–gel and wet impregnation method for their potential applications in photocatalytic processes for environmental applications in water purification to degrade pollutant dyes. The crystalline phase, morphology, optical properties, and chemical composition of the synthesized nanoparticles (NPs) are studied by using X-ray diffraction (XRD), Scanning electron microscopy (SEM), Transmission electron microscopy (TEM), UV–Visible spectroscopy, and Fourier transform infrared spectroscopy (FTIR). The photocatalytic accomplishment of synthesized nanostructures is observed for the degradation of brilliant green (BG). All the synthesized nanostructures exhibited excellent photodegradation activity. The observed rate of degradation of dye is higher with the Co-S doped TiO_2 nanostructures than pure TiO_2.

1. Introduction

The existence of a wide variety of organic components in the industrial wastewater from apparel, paper industries, and textile factories causes shocking environmental pollution. These effluents consist of harmful non-biodegradable materials, carcinogenic and colored pigments detrimental to human beings (Brown and De Vito, 1993; Chen et al., 2010). Even a small amount (below 1 ppm) of dyes can seriously deteriorate the aqueous environment and can be seen in water (Daneshvar et al., 2004; Grzechulska and Morawski, 2002). Therefore, deprivation of colored organic dyes from wastewater is imperative, important, and demands an urgent consideration. Traditionally, adsorption and coagulation are in practice to degrade the organic effluents (Haque et al., 2011; Shi et al., 2007). However, these particles are secondary perilous contaminants, as dyes are only converted into a solid phase from a liquid phase. Thus, supplementary treatments are vital to resolve the problem of secondary contamination (Galindo et al., 2001; Aleboyeh et al., 2003). During the previous few decades, photocatalysis was considered as a capable alternative treatment for water purification (Ayodhya and Veerabhadram, 2018). The photocatalytic reaction includes a photosensitizer (foreign substance) acting as a photocatalyst, put in contact with the target reactants. This is an effective approach widely used as a tool for the disinte-

* Corresponding author.
E-mail addresses: smhafeezkhan@yahoo.com (M. Hafeez), sumeraraja55@gmail.com (S. Afyaz), awais.phy@hu.edu.pk (A. Khalid), pervaiz.pas@gmail.com, pervaiz_pas@yahoo.com (P. Ahmad), mayeenk@sunway.edu.my (M.U. Khandaker), umar.sahibzada@gmail.com (M.U.K. Sahibzada), ikhtiarahmad@gmail.com (I. Ahmad), khanj10@tsinghua.org.cn (J. Khan), f.alhumaydhi@qu.edu.sa (F.A. Alhumaydhi), talhabmb@bgctub.ac.bd (T.B. Emran), abubakridris@hotmail.com (A.M. Idris).
Peer review under responsibility of King Saud University.

Production and hosting by Elsevier

https://doi.org/10.1016/j.jksus.2022.102028
1018-3647/

gration of different harmful materials, comprising aquatic organic pollutants and atmospheric contaminations. It also shows many advantages over conventional wastewater treatment approaches. For example, the complete decay of organic dyes at normal room temperature by this photocatalytic technique can be accomplished within a few hours. Furthermore, organic effluents can be mineralized to comparatively less toxic products (i.e. water and CO_2) without making secondary harmful pollutants, which need secondary treatment (Aramendía et al., 2005; Lee et al., 2017).

TiO_2 is a well-known, widely used photocatalyst during the last few years, due to its low cost, non-toxicity, and high chemical stability (Chen et al., 2010; Bandara et al., 2005). However, the comparatively bulky band gap (for anatase, Eg > 3.2 eV) of TiO_2 limits its applications in the visible light region of the solar system. Furthermore, a greater recombination rate of photo-generated electrons and holes (hþ/e) in TiO_2 causes small quantum yield and reduces photocatalytic activity (Ackermann et al., 2006). Due to these restrictions, various forms of nanomaterials have been furnished by researchers, such as metallic nanostructures (Khalid et al., 2021; Khalid et al., 2021), metal oxides (Khalid et al., 2021; Khalid et al., 2021), and metal sulfides (Salavati-Niasari et al., 2009; Klimov et al., 2000; Ahmad, 2022). Among these nanostructures, metal sulfide nanomaterials have got significant attention due to their unique electronic and optical properties (Czekaj et al., 1988; Spanhel et al., 1987). One of the famous examples of metal sulfides is Cobalt Sulfide. Cobalt normally forms many sulfides having a general formula of CoSx, which earned significant attention because of their potential applications for hydro dearomatization and hydrodesulfurization in various fields (Tao et al., 2007). Co-S NPs have wide applications in capacitors and lithium-ion batteries (Wang et al., 2006; Hillerová and Zdražil, 1989).

Normally, solid-state methods are used to synthesize cobalt sulfide nanostructures (Bahaa et al., 2019). For example, cobalt sulfide can be synthesized by reacting cobalt and sulfur (Ge et al., 2013; Emadi et al., 2012) or the reaction between Co and hydrogen sulfide (Barret and Colson, 1966), or by the reaction of cobalt monoxide with hydrogen sulfide (Emadi et al., 2012; Qian et al., 1999). Toluene thermal process was used for the selective fabrication of Co_9S_8 and CoS_2 by the reaction of cobalt chloride and sodium polysulfide (Zhan et al., 1999; Li et al., 2019). In a hydrazine solution, at 120 °C, CoS was prepared from amorphous cobalt sulfide (Emadi et al., 2012).

Later, hydrothermal method was applied to formulate metal sulfide nanomaterials, having advantages over conventional methods, including low cost, high purity, and desired morphology (Zhan et al., 1999; Salavati-Niasari et al., 2009). The hydrothermal method has been established to fabricate metal sulfides by using thioglycolic acids as a non-toxic template and sulfide source (Zhao et al., 2004). In this report we have synthesized Co-S-TiO_2 nanostructures by applying wet impregnation method using Co $(NO_3)_2{\cdot}6H_2O$ as a source of Co and sodium thiosulphate for sulfur that manifest excellent photocatalytic activity towards dye degradation. BG dye was used to observe the photocatalytic dye degradation behavior of pure and modified TiO_2 nanostructures in UV region. These results will provide improved direction to researchers employed in the fields of environmental remediation and photocatalysis.

2. Results and discussion

2.1. Diffuse reflectance spectroscopy

Diffuse reflectance is measured by coupling the integrating sphere with the λ-35 spectrometer. The integrating sphere is housed in the sample beam of the spectrometer and is used in place of the sample beam detector. It can be used over the wavelength range of 250–1100 nm for either diffuse reflectance or diffuse transmittance. The instrumental detector, external to the sphere, detects the reference beam when light enters the sphere and bounces around used at the detector in diffuse reflectance mode.

Fig. 1 shows the Tauc plot of TiO_2 and Co-S-TiO_2, respectively. The band gap calculated for TiO_2 is 3.26 and 2.44 for Co-S-TiO_2 which shows a remarkable decrease in band gap of Co-doped TiO_2. This is favorable for efficient utilization of visible light and consequently better photocatalytic activity.

2.2. FTIR analysis

FTIR studies were done to analyze the chemical composition, bond type, and functional groups in the compounds. KBr pellets were taken as a standard to record the spectra over the range of 4000–400 cm^{-1}. Absorption of different frequencies was recorded by placing the samples in the path of the IR radiation source.

Information about phase purity and surface functional groups of materials is obtained through this technique. Different peaks were obtained for different functional groups as shown in Fig. 2. The absorption peak in the range of 1620 cm^{-1} and 3350–3500 cm^{-1} could be assigned to the hydroxyl group of water molecules that are absorbed by the sample. Peaks in the range of 400–470 cm^{-1} show metal sulfur bonds. Peaks in the range of 400–1000 cm-^{1} were due to bending and stretching vibrations of M−O bonds. Fig. 3..

2.3. X-ray diffraction analysis

X-ray diffraction is a powerful non-destructive technique for characterizing crystalline materials. It provides data about the structure, preferred crystal orientation (texture), phases, and other structural parameters, such as average grain size, crystallinity, strain, and crystal defects.

XRD pattern of TiO_2 in all samples matched with standard (Joint Committee on Powder Diffraction Standards) JCPDS card No. 01–073-1764, which belongs to anatase TiO_2 structure having tetragonal crystal system. The peaks at 2 theta values 25.36°, 30.82°, 38.09°, 48.17°, 55.05°, 62.9°, and 69.58° can be indexed (101), (121), (004), (200), (211), (204) and (116) diffraction planes. The XRD pattern of Co(x)S(y) is amorphous so cannot be related to a single phase. It can be seen clearly in composites intensity of

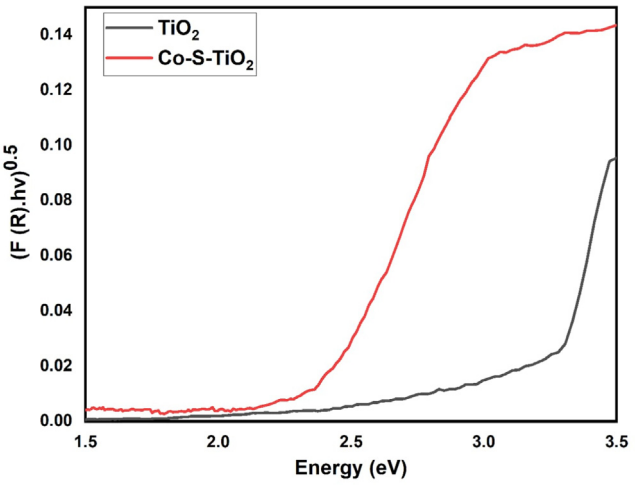

Fig. 1. Tauc plot of TiO_2 and Co-S-TiO_2 for the determination of band gap.

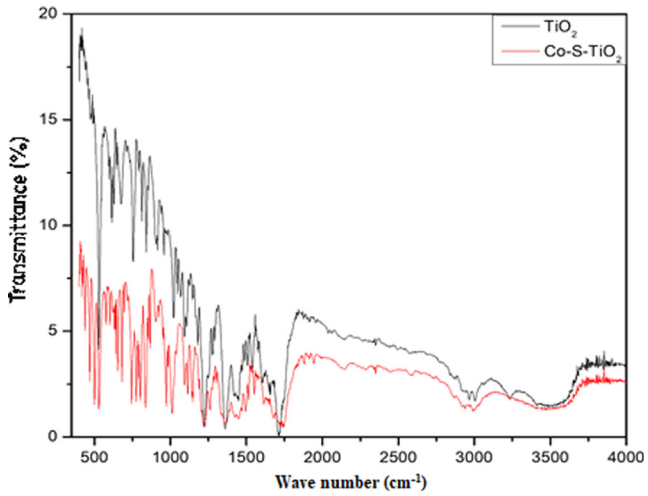

Fig. 2. FTIR Spectrum of TiO_2 and Co-S-TiO_2.

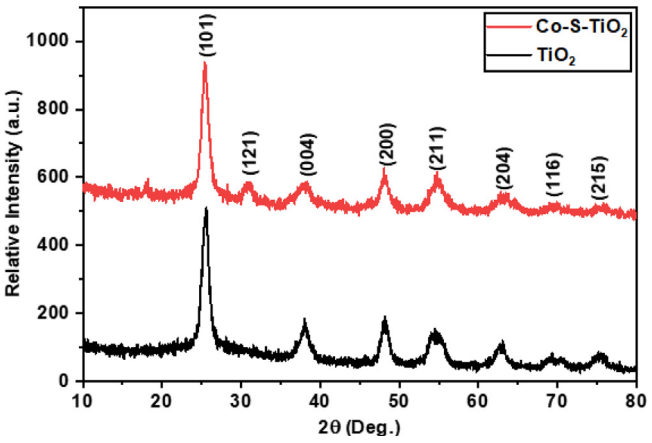

Fig. 3. XRD Spectrum for TiO_2 and Co-S-TiO_2.

peaks decreases on increasing Co-S content, which means the amorphous nature of Co-S also hinders the crystal growth of TiO_2 NPs.

2.4. TEM analysis

TEM analysis was performed on a Field Electron and Ion Company (FEI) Tecnai F20 S-Twin microscope at 200 kV to study morphologies of synthesized nanomaterials. Fig. 4 (a), (b) shows TEM images of prepared samples (TiO_2 and Co-S-TiO_2), respectively. Many NPs can be observed in the images. As the concentration of surfactant increases, the agglomeration of particles decreases, and free-standing particles were being observed. In Fig. 4 (a and b), round ball-like morphologies are depicted. In some regions, there are well-defined boundaries present while in some region's agglomeration occurred.

2.5. SEM analysis

SEM allows the imaging of the topography of a solid surface with the help of backscattered or secondary electrons. Fig. 5 **(a, b)** shows images of synthesized nanostructures obtained from SEM. The observed micrographs to study the morphological characteristics are lying within the range of 50,000 X.

Numerous scientists studied the degradation of dyes in the past few decades. Umabala *et al*., reported the degradation of BG using H_2O_2 sensitized $BiVO_4$ in the visible region of light (Umabala et al., 2016). Shanmugam *et al.*, observed the photocatalytic degradation of BG using undoped and Zn doped SnO_2 NPs under sunlight irradiation (Shanmugam et al., 2016). Razzaq *et al.,* studied dye degradation behavior of TiO_2-NPs using bromophenol blue (BPB) under UV light (Razzaq et al., 2021). Khalid *et al.* evaluated the photodegradation mechanism of methyl orange (MO) by using pure and Fe doped TiO_2 and found that the degradation efficiency in Fe doped TiO_2 is more than TiO_2 alone (Khalid et al., 2021). To investigate the efficiency of the as-prepared catalyst, the photocatalytic degradation of BG was conducted as a model compound to measure the photocatalytic activity of TiO_2 and CoS-TiO_2 composite NPs.

2.6. UV–Visible spectroscopic analysis for photodegradation mechanism

UV–Visible spectroscopy was used to measure the change in the concentration. The change in concentration measures and monitor the activity as a function of irradiation time. The UV–Vis absorption spectra for BG degradation (before and after degradation) by pure TiO_2 and Co-S-TiO_2 at various time intervals are shown in Fig. 6 and Fig. 7. In this study, the BG shows an absorbance peak at 628 nm and is inversely proportional to time (UV irradiation). Results showed that the catalytic efficiency of TiO_2 NPs enhanced considerably with the addition of CoS moiety. All the synthesized samples show good photocatalytic performance by almost completely degrading BG dye in just 70–80 min which is much better performance as compared to commercial Degussa P25 which takes about 110 min to degrade the same dye under the same environment. The photodegradation mechanism of BG dye by pure and Co-S-TiO_2 is since Co and S adsorbed on TiO_2 surface is photoexcited for the generation of electrons and holes in conduction and valence band. An accelerated electron produces a hole (+ve), which

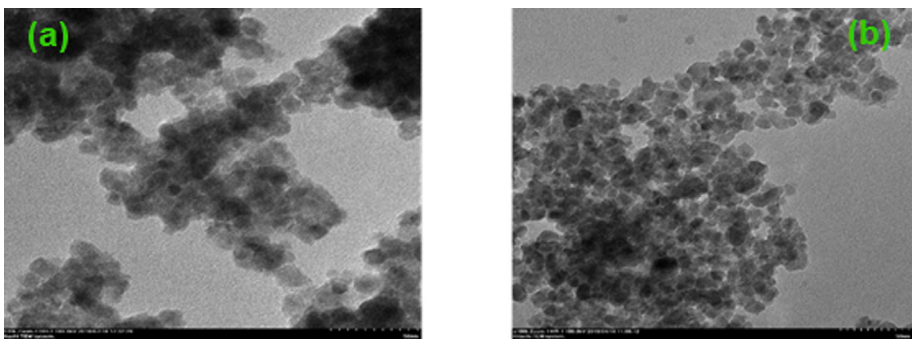

Fig. 4. (a) TEM images of TiO_2 (b) TEM images of Co-S-TiO_2.

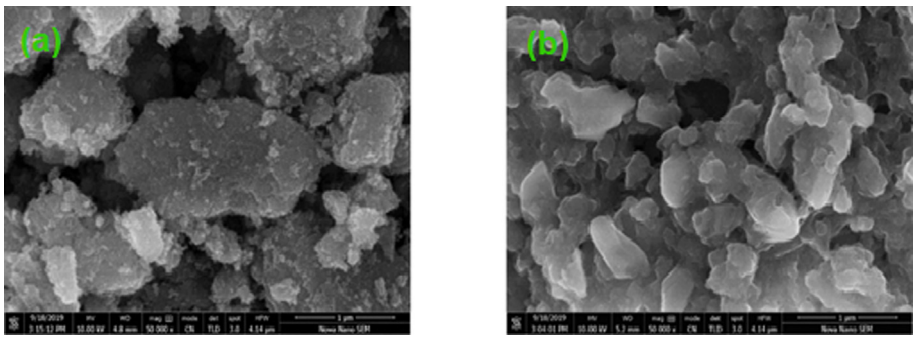

Fig. 5. (a) SEM image of TiO2, (b) SEM image of Co-S-TiO2.

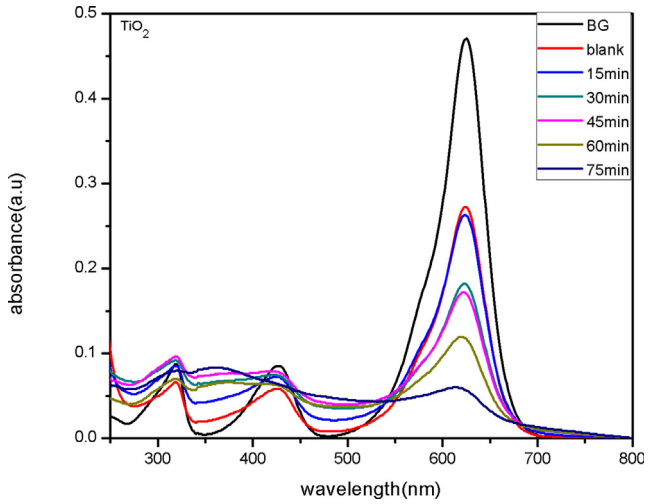

Fig. 6. UV–Visible spectra of Brilliant green solution before and after degradation by TiO_2.

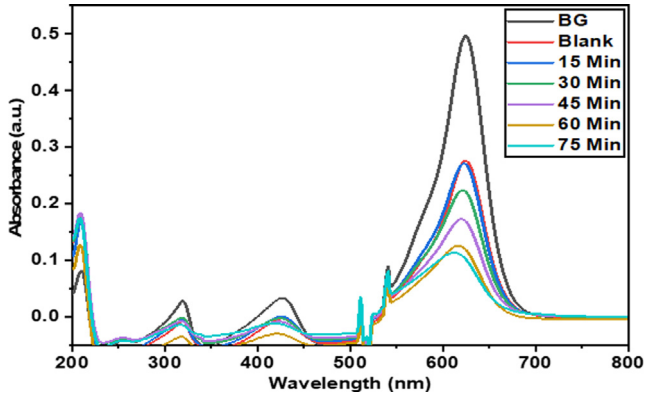

Fig. 7. UV–Vis spectra of Brilliant green solution before and after degradation by Co-S-TiO_2.

reacts with water to produce hydroxyl radicals. These radicals are considered strong oxidizing agents and are responsible for dye degradation (Dlamini et al., 2011). It is indeed conceivable that photogenerated electrons reduce dissolved oxygen, resulting in the creation of the superoxide anion radical. These anion radicals also were potent oxidizers, designed to destroy any ingested organic compounds or nucleic acids lying near the surface of catalysts (Muneer et al., 1997).

The percent degradation rate of BG was measured by the following formula (Ali, 2010).

$$X = \frac{C_0 - C}{C_0} x\ 100 \quad (1)$$

Where.

X = Degree of photo degradation, C_0 = Initial concentration and C = Concentration of dye at time.

Fig. 8 represents the percent degradation of BG dye by TiO_2 and Co-S-TiO_2 at different time intervals. It is clear from the figure that photocatalytic degradation of TiO_2 NPs significantly improved by the addition of different ratios of Co-S. Initially, degradation of dyes was negligible up to 30 min while the solution in dark, after irradiation of visible light, it increased with time and after 75 min maximum degradation was achieved. In the total time interval, the amount of dye degraded was 55 % and 65 % for TiO_2 and Co-S-TiO_2, respectively. Hence Co-S co-doped TiO_2 nanostructures showed greater catalytic activity as compared to pure TiO_2 Photocatalytic activity increases with increasing irradiation time (Sharma et al., 2021) and after 75 min maximum degradation occurred as observed through a UV–Visible spectrophotometer. We know that the surface-to-volume ratio of the nanoparticles (NPs) increases as the crystallite size decreases. Due to size reduction, photo-generated electron/hole pairs can migrate to the surface through a short pathway, and the e-/h + volume recombination rate should drop, resulting in higher photocatalytic activity (Sarkar et al., 2020). The schematic illustration for the complete mechanism of photocatalytic activity by Co-S-TiO_2 is shown in Fig. 9.

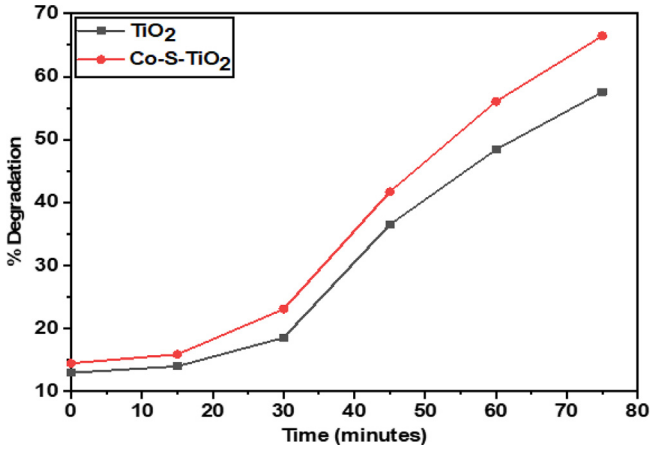

Fig. 8. percent degradation graph of TiO_2 and Co-S-TiO_2.

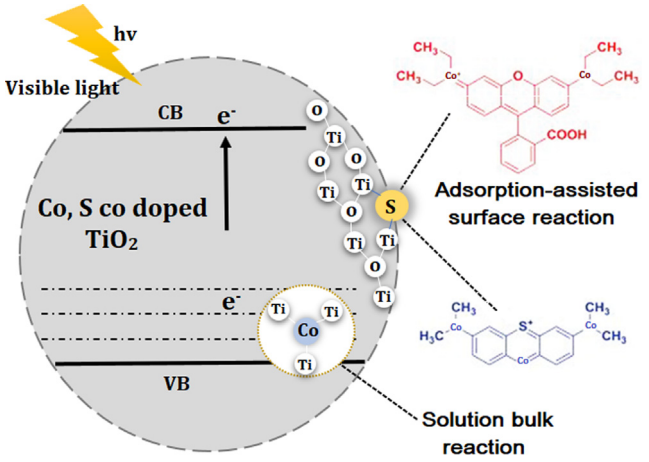

Fig. 9. Schematic illustration for photocatalytic mechanism.

3. Materials and methods

3.1. Chemicals used

The chemicals used were cobalt nitrate hexahydrate (Tech-VNR PROLABO), silicone oil (Sigma Aldrich), titanium isopropoxide (DAEJUNG), thiourea (MERCK), dimethyl sulfoxide (LAB-SCAN), acetic acid (LAB-SCAN), ethanol (Analar), methanol (Analar), distilled water and BG (Sigma Aldrich). All these chemicals were analytical reagent grade.

3.2. Nanostructures synthesis method

Co-S-TiO_2 NPs were prepared by using the wet impregnation method. Nanocrystalline TiO_2 was synthesized by the sol–gel method as described by Choi et al (Choi et al., 2007; Khalid et al., 2022). The sol–gel method was used in the preparation of TiO_2 nanostructures. 0.1 mol of titanium isopropoxide was taken and slowly added into 100 mL of absolute ethanol to form solution 1. Solution 2 was prepared by mixing ethanol, acetic acid, and distilled water (7:3:1). Then, solution 1 was added into solution 2 dropwise under continuous stirring at room temperature. After that, the solution was heated at 50–60 °C until sol is formed, followed by vigorous stirring for 4–6 h, and aged overnight at room temperature to prepare the gel. The resulting gel was dried at 100 °C for 10 h and calcined at 450 °C for 4 h to eliminate the remaining organic impurities and to obtain desired TiO_2 structures. CoS-TiO_2 nanostructures were synthesized by using the wet impregnation method. These nanostructures were produced by refluxing different ratios of cobalt nitrate hexahydrate (2 mmol) thiourea (1 mmol), and nanocrystalline TiO_2 (7.6 mmol) in DMSO (Boiling point 189 °C) at about 220 °C for one hour. The obtained precipitate was centrifuged, washed with methanol, and dried overnight in an oven at 80 to 90 °C to obtain Co-S-TiO_2 nanostructure powder.

3.3. Characterization of synthesized nanostructures

These nanostructures were investigated through X-ray diffraction (XRD) (Azeez et al., 2018), scanning electron microscopy (SEM), diffuse resonance spectroscopy (DRS), Fourier transform infrared spectroscopy (FTIR), and transmission electron microscopy (TEM). Powder X-ray diffraction patterns were recorded with the help of Burker D8 Advance X-ray diffraction using Cu Kα radiation (λ = 1.5418 Å). Transmission electron micrographs were accomplished on a Field Electron and Ion Company (FEI) Tecani G2 F20S-Twin microscope operating on an accelerating voltage at 200 kV. FTIR spectrometer was used, to investigate chemical composition, bond type, and functional groups in the compounds. For recording spectra, Shimazdu-8400S FTIR spectrophotometer was used. KBr pallets were taken as a standard to record the spectra over the range of 400–4000 cm^{-1}.

3.4. Photocatalytic activity of synthesized nanostructures

Photocatalytic activity experiments using the TiO_2 and Co-S-TiO_2 nanostructures were accomplished at room temperature. The nanostructure powders were dispersed in 100 mL of an aqueous solution of BG (1×10^{-5}) in a 100 mL beaker. The mixture was stirred for about 15 min and kept in dark for 40–45 min, to reestablish adsorption–desorption equilibrium. The content was irradiated in sunlight for various time intervals. After a periodic interval, 3 mL of the reaction mixture was taken. The concentration of BG was analyzed by monitoring the absorbance at 623 nm, using a UV–Vis double beam spectrophotometer (Shimazdu 1601PC).

4. Conclusions

In summary visible light photocatalyst TiO_2 and Co-S-TiO_2 were synthesized successfully by sol–gel and thermal decomposition method. The synthesized materials are in both amorphous and crystalline forms shown through XRD. SEM results showed that nanostructures possess round, oval, irregular, and triangular morphologies. TEM results showed ball-like morphologies of synthesized NPs. FT-IR results support the formation of TiO_2 and Co-S-TiO_2 nanostructures. BG was used as a model compound to observe the photocatalytic activity of synthesized nanomaterials in the visible light region. The synthesized nanostructures expressed excellent photocatalytic activity for dyes degradation. In comparison to pure TiO_2 nanostructures, Co-S-TiO_2 nanostructures showed greater catalytic activity. Results showed that Co-S-TiO_2 will be a potential candidate in comparison with pure TiO_2 for water remediation applications. These results will provide improved direction to researchers employed in the fields of environmental remediation and photocatalysis.

Declaration of Interest Statement

The authors declare that they have no known competing financial interests or personal relationships that could have appeared to influence the work reported in this paper.

Acknowledgements

The authors extend their appreciation to the Higher Education Commission of Pakistan (HEC) for providing funds for our research work under the National Research Program for Universities (NRPU) project No 10928.

Funding

The authors extend their appreciation to the Deanship of Scientific Research at King Khalid University for funding this work through Group Research Project under grant number (R.G. P.2/146/43).

References

Brown, M.A., De Vito, S.C., 1993. Predicting azo dye toxicity. Critical reviews in environmental science and technology 23 (3), 249–324.

Chen, S., Zhang, J., Zhang, C., Yue, Q., Li, Y., Li, C., 2010. Equilibrium and kinetic studies of methyl orange and methyl violet adsorption on activated carbon derived from Phragmites australis. Desalination 252 (1-3), 149–156.

Daneshvar, N., Salari, D., Khataee, A., 2004. Photocatalytic degradation of azo dye acid red 14 in water on ZnO as an alternative catalyst to TiO2. Journal of photochemistry and photobiology A: chemistry 162 (2–3), 317–322.

Grzechulska, J., Morawski, A.W., 2002. Photocatalytic decomposition of azo-dye acid black 1 in water over modified titanium dioxide. Applied Catalysis B: Environmental 36 (1), 45–51.

Haque, E., Jun, J.W., Jhung, S.H., 2011. Adsorptive removal of methyl orange and methylene blue from aqueous solution with a metal-organic framework material, iron terephthalate (MOF-235). Journal of Hazardous materials 185 (1), 507–511.

Shi, B., Li, G., Wang, D., Feng, C., Tang, H., 2007. Removal of direct dyes by coagulation: the performance of preformed polymeric aluminum species. Journal of hazardous materials 143 (1-2), 567–574.

Galindo, C., Jacques, P., Kalt, A., 2001. Photooxidation of the phenylazonaphthol AO20 on TiO2: kinetic and mechanistic investigations. Chemosphere 45 (6–7), 997–1005.

Aleboyeh, A., Aleboyeh, H., Moussa, Y., 2003. "Critical" effect of hydrogen peroxide in photochemical oxidative decolorization of dyes: Acid Orange 8, Acid Blue 74 and Methyl Orange. Dyes and pigments 57 (1), 67–75.

Ayodhya, D., Veerabhadram, G., 2018. A review on recent advances in photodegradation of dyes using doped and heterojunction based semiconductor metal sulfide nanostructures for environmental protection. Materials today energy 9, 83–113.

Aramendía, M.A., Marinas, A., Marinas, J.M., Moreno, J.M., Urbano, F.J., 2005. Photocatalytic degradation of herbicide fluroxypyr in aqueous suspension of TiO2. Catalysis Today 101 (3-4), 187–193.

Lee, Y.Y., Moon, J.H., Choi, Y.S., Park, G.O., Jin, M., Jin, L.Y., Li, D., Lee, J.Y., Son, S.U., Kim, J.M., 2017. Visible-light driven photocatalytic degradation of organic dyes over ordered mesoporous Cd x Zn1–x S materials. The Journal of Physical Chemistry C 121 (9), 5137–5144.

Chen, X., Shen, S., Guo, L., Mao, S.S., 2010. Semiconductor-based photocatalytic hydrogen generation. Chemical reviews 110 (11), 6503–6570.

Bandara, J., Udawatta, C., Rajapakse, C., 2005. Highly stable CuO incorporated TiO 2 catalyst for photocatalytic hydrogen production from H2O. Photochemical & Photobiological Sciences 4 (11), 857–861.

Ackermann, L., Spatz, J.H., Gschrei, C.J., Born, R., Althammer, A., 2006. A Diaminochlorophosphine for Palladium-Catalyzed Arylations of Amines and Ketones. Angewandte Chemie International Edition 45 (45), 7627–7630.

Khalid, A., Ahmad, P., Alharthi, A.I., Muhammad, S., Khandaker, M.U., Rehman, M., Faruque, M.R.I., Din, I.U., Alotaibi, M.A., Alzimami, K., Bradley, D.A., 2021. Structural, optical and antibacterial efficacy of pure and zinc-doped copper oxide against pathogenic bacteria. Nanomaterials 11 (2), 451.

Khalid, A., Ahmad, P., Alharthi, A.I., Muhammad, S., Khandaker, M.U., Faruque, M.R.I., Din, I.U., Alotaibi, M.A., Khan, A., Bakhsheshi-Rad, H.R., 2021. Synergistic effects of Cu-doped ZnO nanoantibiotic against Gram-positive bacterial strains. Plos one 16 (5).

Khalid, A., Ahmad, P., Alharthi, A.I., Muhammad, S., Khandaker, M.U., Faruque, M.R.I., Khan, A., Din, I.U., Alotaibi, M.A., Alzimami, K., Alfuraih, A.A., Bradley, D.A., 2021. Enhanced Optical and Antibacterial Activity of Hydrothermally Synthesized Cobalt-Doped Zinc Oxide Cylindrical Microcrystals. Materials 14 (12), 3223.

Khalid, A., Ahmad, P., Alharthi, A.I., Muhammad, S., Khandaker, M.U., Iqbal Faruque, M.R., Din, I.U., Alotaibi, M.A., 2021. Unmodified titanium dioxide nanoparticles as a potential contrast agent in photon emission computed tomography. Crystals 11 (2), 171.

Salavati-Niasari, M., Loghman-Estarki, M.R., Davar, F., 2009. Controllable synthesis of wurtzite ZnS nanorods through simple hydrothermal method in the presence of thioglycolic acid. Journal of Alloys and compounds 475 (1–2), 782–788.

Klimov, V.I., Mikhailovsky, A.A., Xu, S.u., Malko, A., Hollingsworth, J.A., Leatherdale, C.A., Eisler, H.-J., Bawendi, M.G., 2000. Optical gain and stimulated emission in nanocrystal quantum dots. science 290 (5490), 314–317.

Ahmad, P. et al., 2022. The antibacterial and antioxidant efficacy and neutron sensing potency of 10B enriched hexagonal boron nitride nanoparticles. Materials Science in Semiconductor Processing 141, 106419.

Czekaj, C.L., Rau, M.S., Geoffroy, G.L., Guiton, T.A., Pantano, C.G., 1988. An organometallic route to micron-sized whiskers of zinc sulfide. Inorganic Chemistry 27 (19), 3267–3269.

Spanhel, L., Haase, M., Weller, H., Henglein, A., 1987. Photochemistry of colloidal semiconductors. 20. Surface modification and stability of strong luminescing CdS particles. Journal of the American Chemical Society 109 (19), 5649–5655.

Tao, F., Zhao, Y.-Q., Zhang, G.-Q., Li, H.-L., 2007. Electrochemical characterization on cobalt sulfide for electrochemical supercapacitors. Electrochemistry Communications 9 (6), 1282–1287.

Wang, J., Ng, S.H., Wang, G.X., Chen, J., Zhao, L., Chen, Y., Liu, H.K., 2006. Synthesis and characterization of nanosize cobalt sulfide for rechargeable lithium batteries. Journal of power sources 159 (1), 287–290.

Hillerová, E., Zdražil, M., 1989. Activity and selectivity of carbon-supported transition metal sulfides in simultaneous hydrodearomatization and hydrodesulfurization. Collection of Czechoslovak chemical communications 54 (10), 2648–2656.

Bahaa, A., Balamurugan, J., Kim, N.H., Lee, J.H., 2019. Metal–organic framework derived hierarchical copper cobalt sulfide nanosheet arrays for high-performance solid-state asymmetric supercapacitors. Journal of Materials Chemistry A 7 (14), 8620–8632.

Ge, W., Kawahara, K., Tsuji, M., Ago, H., 2013. Large-scale synthesis of NbS 2 nanosheets with controlled orientation on graphene by ambient pressure CVD. Nanoscale 5 (13), 5773.

Emadi, H., Salavati-Niasari, M., Davar, F., 2012. Synthesis and characterization of cobalt sulfide nanocrystals in the presence of thioglycolic acid via a simple hydrothermal method. Polyhedron 31 (1), 438–442.

Barret, P., J. Colson, and D. D, *MECANISME DE LA SULFURATION DOXYDES METALLIQUES PAR LE GAZ SULFHYDRIQUE*. COMPTES RENDUS HEBDOMADAIRES DES SEANCES DE L ACADEMIE DES SCIENCES SERIE C, 1966. **262**(1): p. 83-&.

Qian, X.F., Zhang, X.M., Wang, C., Xie, Y., Qian, Y.T., 1999. The preparation and phase transformation of nanocrystalline cobalt sulfides via a toluene thermal process. Inorganic Chemistry 38 (11), 2621–2623.

Zhan, J.H., Xie, Y., Yang, X.G., Zhang, W.X., Qian, Y.T., 1999. Hydrazine-assisted low-temperature hydrothermal preparation of nanocrystalline Jaipurite. Journal of Solid State Chemistry 146 (1), 36–38.

Li, L., Ding, Y., Huang, H., Yu, D., Zhang, S., Chen, H.-Y., Ramakrishna, S., Peng, S., 2019. Controlled synthesis of unique Co9S8 nanostructures with carbon coating as advanced electrode for solid-state asymmetric supercapacitors. Journal of colloid and interface science 540, 389–397.

Salavati-Niasari, M., Ghanbari, D., Davar, F., 2009. Synthesis of different morphologies of bismuth sulfide nanostructures via hydrothermal process in the presence of thioglycolic acid. Journal of Alloys and Compounds 488 (1), 442–447.

Zhao, Y., Zhang, Y., Zhu, H., Hadjipanayis, G.C., Xiao, J.Q., 2004. Low-temperature synthesis of hexagonal (wurtzite) ZnS nanocrystals. Journal of the American Chemical Society 126 (22), 6874–6875.

Umabala, A., Suresh, P., Rao, A.P., 2016. Effective visible light photocatalytic degradation of Brilliant green using H2O2 sensitized BiVO4. Der Pharma Chemica 8, 61–66.

Shanmugam, N., Sathya, T., Viruthagiri, G., Kalyanasundaram, C., Gobi, R., Ragupathy, S., 2016. Photocatalytic degradation of brilliant green using undoped and Zn doped SnO2 nanoparticles under sunlight irradiation. Applied Surface Science 360, 283–290.

Razzaq, Z., Khalid, A., Ahmad, P., Farooq, M., Khandaker, M.U., Sulieman, A., Rehman, I.U., Shakeel, S., Khan, A., 2021. Photocatalytic and Antibacterial Potency of Titanium Dioxide Nanoparticles: A Cost-Effective and Environmentally Friendly Media for Treatment of Air and Wastewater. Catalysts 11 (6), 709.

Khalid, A., Ahmad, P., Alharth, A.I., Muhammad, S., Khandaker, M.U., Faruque, M.R.I., Din, I.U., Alotaibi, M.A., 2021. A practical method for incorporation of Fe (III) in Titania matrix for photocatalytic applications. Materials Research Express 8 (4), 045006.

Dlamini, L.N., Krause, R.W., Kulkarni, G.U., Durbach, S.H., 2011. Photodegradation of bromophenol blue with fluorinated TiO2 composite. Applied Water Science 1 (1-2), 19–24.

Muneer, M., Philip, R., Das, S., 1997. Photocatalytic degradation of waste water pollutants. Titanium dioxidemediated oxidation of a textile dye, Acid Blue 40. Research on Chemical Intermediates 23 (3), 233–246.

Ali, H., 2010. Biodegradation of synthetic dyes—a review. Water, Air, & Soil Pollution 213 (1), 251–273.

Sharma, R., Saini, H., Paul, D.R., Chaudhary, S., Nehra, S.P., 2021. Removal of organic dyes from wastewater using Eichhornia crassipes: a potential phytoremediation option. Environmental Science and Pollution Research 28 (6), 7116–7122.

Sarkar, S., Ponce, N.T., Banerjee, A., Bandopadhyay, R., Rajendran, S., Lichtfouse, E., 2020. Green polymeric nanomaterials for the photocatalytic degradation of dyes: a review. Environmental Chemistry Letters 18 (5), 1569–1580.

Choi, H., Stathatos, E., Dionysiou, D.D., 2007. Photocatalytic TiO2 films and membranes for the development of efficient wastewater treatment and reuse systems. Desalination 202 (1–3), 199–206.

Khalid, A., Ahmad, P., Khan, A., Khandaker, M.U., Kebaili, I., Alam, M.M., Din, I.U., Muhammad, S., Razzaq, Z., Rehman, I.U., Abbasi, H.A., Hayat, D., 2022. *Cytotoxic and Photocatalytic Studies of Hexagonal Boron Nitride Nanotubes: A potential Candidate for Wastewater and Air Treatment.* RSC. Advances 12 (11), 6592–6600.

Azeez, F., Al-Hetlani, E., Arafa, M., Abdelmonem, Y., Nazeer, A.A., Amin, M.O., Madkour, M., 2018. The effect of surface charge on photocatalytic degradation of methylene blue dye using chargeable titania nanoparticles. Scientific reports 8 (1).